

A Scaling Theory for Atmospheric Heat Redistribution on Rocky Exoplanets.

DANIEL D.B. KOLL

Department of Earth, Atmospheric and Planetary Sciences, MIT, Cambridge, MA 02139, USA

ABSTRACT

Atmospheric heat redistribution shapes the remote appearance of rocky exoplanets but there is currently no easy way to predict a planet’s heat redistribution from its physical properties. In this paper I derive an analytical scaling theory for the heat redistribution on tidally locked rocky exoplanets. The main parameters of the theory are a planet’s equilibrium temperature, its surface pressure, and its broadband longwave optical thickness. I validate the theory against general circulation model simulations of TRAPPIST-1b, GJ1132b, and LHS 3844b. I find that heat redistribution becomes efficient, and a planet’s observable thermal phase curve and secondary eclipse start to deviate significantly from that of a bare rock, once surface pressure exceeds $\mathcal{O}(1)$ bar. These results thus bridge the gap between theory and imminent observations with the *James Webb Space Telescope*. They can also be used to parameterize the effect of 3D atmospheric dynamics in 1D models, thereby improving the self-consistency of such models.

Keywords: planets and satellites: atmospheres — planets and satellites: terrestrial planets — planets and satellites: individual (GJ 1132 b, LHS 3844 b, TRAPPIST-1 b, LHS 1140 b, 55 Cnc e, WASP-47 b, HD 219134 b, HD 15337 b, L 98-59 b, HD 213885 b, TOI-270 b, GL 357 b)

1. INTRODUCTION

Telescope observations have recently begun to probe the atmospheres of small, rocky, exoplanets around nearby stars (Demory et al. 2016; de Wit et al. 2018; Diamond-Lowe et al. 2018, Kreidberg et al, submitted). These observations will only get better in the near future with the launch of the *James Webb Space Telescope* (*JWST*) and the construction of extremely large ground-based telescopes. The data that we will be able to obtain with these instruments promise insight into fundamental questions such as how rocky exoplanets form, how many of them host atmospheres, and whether any of them might be habitable.

To interpret these observations correctly, however, we need to understand the chemical and physical processes that shape the observable features of rocky exoplanets. These processes include radiative transfer and molecular absorption (Seager & Sasselov 2000), gas-phase chemistry (Moses et al. 2011; Hu & Seager 2014), clouds and hazes (Hörst et al. 2018; Moran et al. 2018), as well

as large-scale atmospheric dynamics (Joshi et al. 1997; Merlis & Schneider 2010). Of these processes atmospheric dynamics has an outsized impact on thermal observations, because it determines a planet’s global heat redistribution which sets the depth of the planet’s secondary eclipse as well as the shape of the planet’s thermal phase curve.

Unfortunately heat redistribution remains poorly represented in most models that are being used to match and interpret exoplanet observations. The underlying reason is that these retrieval models have to be fast enough to be run $\sim 10^5 - 10^6$ times (Madhusudhan & Seager 2009; Line et al. 2013), which is required to comprehensively map out which atmospheric scenarios can, or cannot, fit an observed dataset. As a consequence most retrieval models are idealized one-dimensional representations of a planet’s atmosphere (e.g., Tinetti et al. 2007; Madhusudhan & Seager 2009; Benneke & Seager 2012; Line et al. 2013; Kempton et al. 2017). By virtue of being 1D, these models cannot resolve 3D processes such as clouds and atmospheric heat redistribution, which has been shown to bias the results of atmospheric retrievals as well as model mean states (Line & Parmentier 2016; Feng et al. 2016; Fauchez et al. 2018).

In principle 3D processes including atmospheric heat redistribution can be resolved by more complex models, such as general circulation models (GCMs). In practice 3D models are computationally far too costly to be used in place of 1D retrieval models. For example, the GCM used later in this paper requires about 24 hours of computation time on 8 processors. Even a dedicated supercomputer, running 32 GCM simulations in parallel for an entire month, would thus only be able to explore $\sim 10^3$ parameter combinations, falling far short of being useful for standard retrieval techniques.

An important question is therefore how exoplanet retrieval models should represent the basic physics that determines observable quantities such as a planet’s day-side emission or its thermal phase curve, while remaining computationally cheap. Most 1D models represent the effects of heat redistribution by adjusting the planet’s dayside energy budget, which can be written as (Burrrows 2014)

$$T_{day} = T_* \sqrt{\frac{R_*}{d}} (1 - \alpha_B)^{1/4} f^{1/4}. \quad (1)$$

Here T_{day} is the dayside brightness temperature¹, T_* is the stellar temperature, R_* is the stellar radius, d is the planet’s semi-major axis, α_B is the planet’s bond albedo, and f is the so-called heat redistribution factor. The redistribution factor f has to lie between 2/3 for a planet without an atmosphere and 1/4 for a planet that is extremely efficient at redistributing heat, but currently there no easy way of expressing f in terms of a planet’s physical properties.

The goal of this paper is to develop a simple scaling theory for f . I derive the scaling in Section 2. The scaling shows that f is mainly sensitive to a planet’s equilibrium temperature, surface pressure, and its broadband optical thickness (note that the theory also describes the dependency on other physical parameters). I test the theory in Section 3 against GCM simulations of three nearby rocky planets: TRAPPIST-1b, GJ1132b, and LHS3844b (Gillon et al. 2016; Delrez et al. 2018; Berta-Thompson et al. 2015; Vanderspek et al. 2019), which are among the highest-priority targets for upcoming thermal observations with *JWST*. I find that the theory successfully captures the dominant processes that determine atmospheric heat redistribution on these planets. The theory therefore lends insight into the atmospheric dynamics of tidally locked planets. Moreover, it can also be used as a computationally efficient param-

eterization of large-scale dynamics in 1D models, which collaborators and I have recently adopted in a number of related studies (Koll et al; Malik et al; Mansfield et al; Kreidberg et al; all submitted). Because the derivation and GCM simulations assume idealized semi-grey radiative transfer, I take up in Section 4 how this work can be applied to real gases with non-grey absorption. I discuss the results in Section 5 and conclude in Section 6.

2. A SCALING FOR ATMOSPHERIC HEAT REDISTRIBUTION

In this section I first derive an asymptotic solution for a planet’s day-night heat redistribution in the limit of a thin atmosphere. I then use an Ansatz to extend the solution to arbitrary atmospheric thickness, which I will later verify by comparing theory against GCM simulations.

Due to the relatively slow rotation of tidally locked planets, the nightside atmosphere is in weak-temperature-gradient (WTG) balance (Pierrehumbert 2011; Mills & Abbot 2013). WTG balance states that the rate at which parcels of air radiatively cool to space is equal to the rate at which they sink and are warmed by adiabatic compression. Using the grey optical depth τ as the vertical coordinate, this balance can be written as (see Koll & Abbot 2016)

$$\frac{c_p \omega}{g} \left(\frac{dT}{d\tau} - \beta \frac{T}{\tau} \right) = \frac{dF}{d\tau}. \quad (2)$$

Here $T(\tau)$ is the atmosphere’s nightside vertical temperature profile, $F(\tau)$ is the net infrared flux, ω is the vertical velocity induced by the large-scale atmospheric circulation, c_p is the atmosphere’s specific heat capacity, g is the acceleration of gravity, $\beta \equiv R/(c_p n_{LW})$ is the dry adiabatic lapse rate in optical depth coordinates, R is the atmosphere’s specific heat constant, and $n_{LW} = 1$ if opacity is independent of pressure (e.g., if molecular line widths are set by thermal broadening) while $n_{LW} = 2$ for pressure broadening. For sinking air $\omega > 0$.

If one evaluates F at the top-of-atmosphere one obtains the nightside’s outgoing longwave radiation, which in equilibrium has to be equal to the day-night heat transport by the atmosphere. I will call this nightside flux of outgoing longwave radiation F_n .

The nightside flux F_n is set by three processes: radiation, which sets how quickly sinking air radiates energy to space, large-scale subsidence, which sets how long air sinks before it gets moved back to the dayside, and the stellar irradiation received by the planet, which sets how

¹ T_{day} is hotter than the average dayside temperature because the observer viewing geometry is skewed towards the hot substellar point (Cowan & Agol 2008).

much heat there is for air to radiate to space in the first place. Any of these processes can individually limit F_n , so I search for a separable solution of the form

$$F_n = \hat{f}(\tau_{LW}) \times \hat{g}(p_s, \dots) \times \sigma T_{eq}^4, \quad (3)$$

where τ_{LW} is the optical thickness, p_s is the surface pressure, and T_{eq} is the planet's equilibrium temperature.

To constrain \hat{f} I consider the limit of a vanishingly thin atmosphere. For an optically thin column of air it is well-known that the column's radiative cooling is linearly proportional to the column's optical thickness (Pierrehumbert 2010), so $\hat{f}(\tau_{LW}) \approx \tau_{LW}$.

To constrain \hat{g} I scale the WTG equation. In the limit of a vanishingly thin atmosphere the nightside becomes roughly isothermal and approaches the grey skin temperature, so $T(\tau) \approx T_{skin} = 2^{-1/4} T_{eq}$ (Wordsworth 2015). Neglecting the dependence on τ , which is already captured by \hat{f} , the WTG equation then implies $F_n \sim \beta T_{skin} c_p \omega / g$. The only unknown in this relation is ω , which is set by the atmosphere's large-scale dynamics. Koll & Abbot (2016) showed that the atmospheric circulations of rocky planets closely resemble heat engines, in which case the sinking velocity is

$$\omega = \chi \frac{p_s}{a} \left(\eta \frac{2R\sigma T_{eq}^5}{C_d p_s} \right)^{1/3}, \quad (4)$$

where χ is a inefficiency factor (which I will determine numerically), a is the planet's radius, η is the heat engine's Carnot efficiency, and C_d is a nondimensional surface drag coefficient. Combining the above expressions, the atmospheric heat transport of a thin atmosphere is equal to

$$F_n = \hat{f}(\tau_{LW}) \times \hat{g}(p_s, \dots) \times \sigma T_{eq}^4, \quad (5)$$

$$= \tau_{LW} \times \frac{\tilde{\chi} \beta c_p}{ag} \left(\frac{R\eta}{C_d} \right)^{1/3} \left(\frac{p_s}{\sigma T_{eq}^2} \right)^{2/3} \times \sigma T_{eq}^4, \quad (6)$$

where I have absorbed all numerical constants into the inefficiency factor χ .

Next, I extend the asymptotic solution in Equation 6 using an Ansatz. To do so note that Equation 6 cannot be generally valid because it predicts that $F_n \rightarrow \infty$ as p_s or τ_{LW} become large, whereas energy conservation requires that $F_n \rightarrow \sigma T_{eq}^4$ for a thick atmosphere. A general solution needs to reduce to the asymptotic solution as p_s and τ_{LW} become small, but tend towards σT_{eq}^4 as one or both parameters become large. I find the following expression satisfies both requirements:

$$F_n = \frac{\hat{f}(\tau_{LW}) \hat{g}(p_s, \dots)}{1 + \hat{f}(\tau_{LW}) \hat{g}(p_s, \dots)} \sigma T_{eq}^4. \quad (7)$$

There is no guarantee that Equation 7 will be exact when $\hat{f}(\tau_{LW}) \hat{g}(p_s, \dots)$ is of order unity. Nevertheless, because it reduces to the correct limits for both a thin and a thick atmosphere, it is physically motivated. Below I compare this solution to GCM simulations and find that it performs well over a wide range of atmospheric parameters.

To transform F_n into a prediction for the observed dayside flux F_d one can use the planet's energy budget, but additionally has to account for an observer's skewed viewing geometry (Cowan & Agol 2008). At secondary eclipse the observer's view is weighted towards the substellar point, which directly faces the observer, and is less sensitive to regions that lie close to the terminator, which tilt away from the observer. The limiting expressions for the flux that an observer sees are $F_d = 8/3 \times \sigma T_{eq}^4$ for a bare rock, and $F_d = \sigma T_{eq}^4$ for a planet with uniform heat redistribution. I therefore write the observed dayside flux as

$$F_d = \left(\frac{8}{3} - \frac{5}{3} \frac{\tau_{LW} \left(\frac{p_s}{1\text{bar}} \right)^{2/3} \left(\frac{T_{eq}}{600\text{K}} \right)^{-4/3}}{k + \tau_{LW} \left(\frac{p_s}{1\text{bar}} \right)^{2/3} \left(\frac{T_{eq}}{600\text{K}} \right)^{-4/3}} \right) \sigma T_{eq}^4 \quad (8)$$

Here $k = ag/(\tilde{\chi} \beta c_p) \times (C_d \sigma^2 / (R\eta))^{1/3} (1\text{bar})^{-2/3} (600\text{K})^{4/3}$ captures all planetary parameters other than the optical thickness, surface pressure, and equilibrium temperature. As I show below, k is of order unity and varies little between most planetary scenarios (e.g., radius and surface gravity tend to vary by less than a factor of two between different rocky planets). I therefore separate k out to underline the dominant dependency of heat redistribution on p_s , τ_{LW} , and T_{eq} . To relate the main result back to the heat redistribution factor f used in 1D models, one can also express it as

$$f = \frac{2}{3} - \frac{5}{12} \times \frac{\tau_{LW} \left(\frac{p_s}{1\text{bar}} \right)^{2/3} \left(\frac{T_{eq}}{600\text{K}} \right)^{-4/3}}{k + \tau_{LW} \left(\frac{p_s}{1\text{bar}} \right)^{2/3} \left(\frac{T_{eq}}{600\text{K}} \right)^{-4/3}}. \quad (9)$$

As expected, Equation 9 recovers the no-redistribution limit $f \rightarrow 2/3$ as $\tau_{LW}, p_s \rightarrow 0$, and the uniform-redistribution limit $f \rightarrow 1/4$ as $\tau_{LW}, p_s \rightarrow \infty$.

3. TESTING THEORY WITH GCM SIMULATIONS

3.1. Numerical setup

To test the analytical theory I use the Flexible Model System (FMS) general circulation model (GCM) with dry thermodynamics. FMS is a widely-used model which has previously been applied to the atmospheres of Earth (Frierson et al. 2006), Jupiter (Liu et al. 2011),

Table 1. Planetary parameters for the GCM simulations.

| | Radius | Period | Surf. gravity | T_{eq}^a |
|-------------|----------------|--------|-------------------|------------|
| | (R_\oplus) | (d) | (m/s^2) | (K) |
| TRAPPIST-1b | 1.12 | 1.51 | 7.95 | 391 |
| GJ1132b | 1.16 | 1.63 | 11.8 | 578 |
| LHS3844b | 1.32 | 0.46 | 12.9 ^b | 805 |

^aEquilibrium temperature, for uniform heat redistribution and zero albedo.

^bAssuming $2.3 M_\oplus$, based on [Chen & Kipping \(2017\)](#).

hot Jupiters ([Heng et al. 2011](#)), tidally locked terrestrial planets ([Merlis & Schneider 2010](#); [Mills & Abbot 2013](#); [Koll & Abbot 2015, 2016](#)), as well as rapidly rotating terrestrial planets ([Kaspi & Showman 2015](#)). Consistent with dry thermodynamics, I do not consider the radiative impact of clouds or photochemical hazes. I discuss the potential shortcomings of these modeling assumptions in Section 5.

The FMS version I use simulates the atmosphere’s full large-scale dynamics coupled to semi-grey (shortwave versus longwave) radiative transfer. Convection is parameterized as instantaneous dry convective adjustment. Near-surface turbulence is parametrized using a standard Monin-Obukhov scheme which self-consistently computes the depth of the boundary layer as well as turbulent diffusion of heat and momentum. The surface is represented by a “slab layer”, that is a single layer with uniform temperature and fixed layer depth. Simulations are all tidally locked and orbits are assumed to be circular so that the stellar flux is fixed in space and constant in time.

I do not include atmospheric shortwave absorption, so all stellar energy is absorbed at the planet’s surface. The planet’s surface albedo is set to zero. Similar to [Friereson et al. \(2006\)](#) I assume the longwave optical thickness depends quadratically on pressure in the lower atmosphere, which represents the effects of pressure broadening, while it depends linearly on pressure in the upper atmosphere, which represents the effect of thermal broadening and helps ensure that the stratosphere equilibrates within reasonable run times.

I use a horizontal resolution of T42, equivalent to about 64×128 points in latitude and longitude, and 30 vertical levels. As is standard in GCMs, FMS includes horizontal hyperdiffusion which acts as a kinetic energy filter at the smallest length scales resolved by the model. Although such a filter can be potentially problematic in

modeling gas giant atmospheres, because the physical processes that lead to frictional dissipation in gas giants are often not explicitly modeled and thus hyperdiffusion acts as a stand-in for unresolved physics ([Koll & Komacek 2018](#)), this issue is less important for rocky planets where friction from the solid surface is captured by the Monin-Obukhov boundary layer scheme.

I simulate three rocky planets that orbit nearby M-dwarfs: TRAPPIST-1b, GJ1132b, and LHS3844b. The planetary parameters are shown in Table 1. The three planets span a wide range of equilibrium temperatures, which is one of the dominant parameters in the theory (Section 2). In addition, the three planets span different rotational regimes. LHS3844b has an orbital period of about 11h, whereas TRAPPIST-1b and GJ1132b have orbital periods of 1.5 and 1.6 days, which translates into a nondimensional Rossby deformation radius of $a/L_{Ro} \approx 3$ for LHS3844b versus $a/L_{Ro} \approx 2$ for TRAPPIST-1b and GJ1132b ([Koll & Abbot 2015](#)). Given that the theoretical scaling does not account for the effect of planetary rotation, comparison between the three planets also provides a check on whether the theory is robust to changes in planetary rotation.

Consistent with the CFL criterion, I find that the simulations are more likely to crash at higher stellar fluxes. I therefore use a numerical diffusion coefficient of $2.31 \times 10^5 \text{ s}^{-1}$ (damping time of half a day) for TRAPPIST-1b and GJ1132b, and between 9.26×10^4 to $2.31 \times 10^4 \text{ s}^{-1}$ for LHS3844b. In some cases I also need to reduce the timestep at low surface pressure or high optical thickness. The default timestep is 120 s for TRAPPIST-1b, 60 s for GJ1132b, and 20 s for LHS3844b.

I simulate the effect on the atmosphere’s heat redistribution of varying atmospheric surface pressure p_s and optical thickness τ_{LW} . I explore a wide combination of both parameters by simulating surface pressures between 0.01 bar and 100 bar, and longwave optical thickness equal to 0.1, 1, and 5. Motivated by the observation that solar system atmospheres have broadband optical thicknesses of about 1-10 at 1 bar ([Robinson & Catling 2014](#)), I also consider a scenario in which I linearly increase optical thickness τ_{LW} with surface pressure p_s using the relation $\tau_{LW} = p_s/1 \text{ bar}$.

3.2. GCM results

Figure 1 shows that thermal phase curves start to significantly deviate from a bare rock once surface pressure exceeds about 1 bar, in agreement with the analytical scaling. Shown are results for simulations with constant optical thickness, $\tau_{LW} = 1$. I compute the thermal phase curves across the *JWST* MIRI bandpass

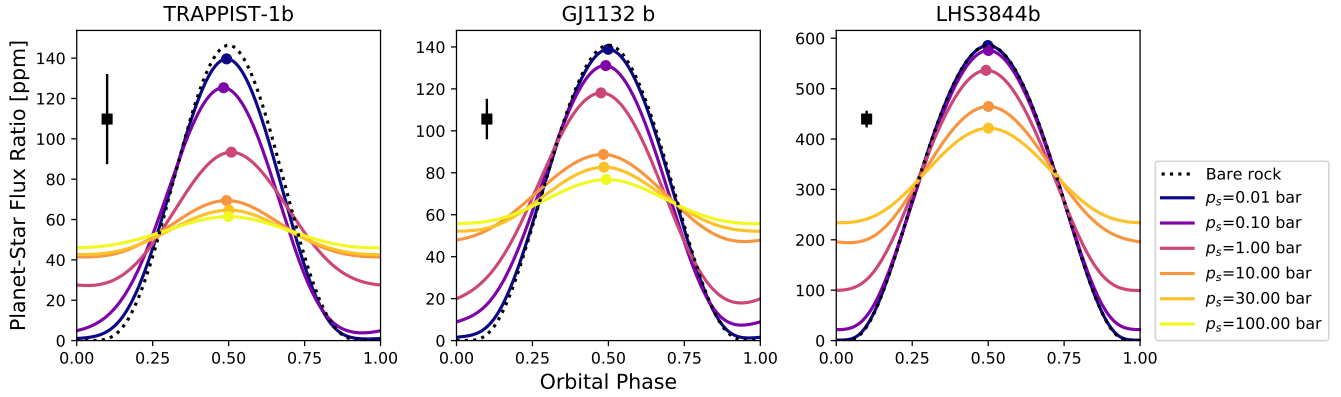


Figure 1. Dayside emission starts to significantly deviate from that of a bare rock once surface pressure exceeds $\mathcal{O}(1)$ bar. Lines show simulated phase curves, and circles show hot spots (i.e., a planet’s maximum thermal emission). Hot spot offsets are negligible and all hot spots remain close to secondary eclipse at orbital phase = 0.5. Black error bars show a lower bound for the 1σ photometric precision possible with *JWST*’s MIRI instrument (photon noise integrated as long as the duration of each planet’s transit), so the planets’ day-night thermal variations should be observable for all three targets.

(5–12 μ m). To convert a planet’s simulated thermal emission to a planet-star flux ratio I assume a blackbody spectrum for the host star. At surface pressures of 0.1 bar or less phase curves are effectively indistinguishable from a bare rock. This is particularly the case once I account for *JWST*’s instrumental precision, which cannot be any better than the photon noise limit but could optimistically be comparable to it (Fig. 1). Conversely, at surface pressures above 10 bar phase curves become increasingly uniform. This matches the theoretical prediction that the transition between a bare rock and a uniform planet happens at $\mathcal{O}(1)$ bar (Eqn. 8). Moreover, for a fixed surface pressure, LHS3844b has the least efficient redistribution while TRAPPIST-1b has the most efficient redistribution. This matches the expectation that, at fixed surface pressure, redistribution is inversely proportional to equilibrium temperature.

Figure 2 compares the theoretical prediction against the dayside brightness temperatures that an observer would see at secondary eclipse. To evaluate k in Equation 9 I assume a high mean-molecular-weight (MMW) atmosphere with $(R, c_p) = (R_{N_2}, c_{p,N_2})$. The Carnot efficiency of a planet with a thin atmosphere is $\eta = 0.3$, and $C_d = 1.9 \times 10^{-3}$ (Koll & Abbot 2016). Koll & Abbot (2016) found numerically that $\chi \approx 0.05$. Based on the numerical experiments here I use $\tilde{\chi} = 0.25$, keeping in mind that $\tilde{\chi}$ is uncertain by about a factor of two due to uncertainty in the heat engine efficiency. As expected, explicit evaluation shows that k is roughly constant, with $k = 1.5$ for TRAPPIST-1b, $k = 2.3$ for GJ1132b, and $k = 2.8$ for LHS3844b.

Figure 2 shows that the scaling correctly captures the main variation in dayside thermal emission across several orders of magnitude variation in surface pressure,

and more than one order of magnitude variation in optical thickness. The scaling is not perfect, however. For example, the scaling tends to slightly overpredict thermal emission at low optical thickness, while it underpredicts thermal emission at high optical thickness. This implies that day-night redistribution is less sensitive to changes in τ_{LW} than is implied by the Ansatz (Eqn. 7). The scaling also does not perfectly capture how dayside thermal emission responds to a increase in surface pressure. In some cases it overpredicts the response (e.g., for TRAPPIST-1b at $\tau_{LW} = 0.1$) while other cases it underpredicts the response (e.g., for LHS3844b at $\tau_{LW} = 5$).

Nevertheless, the majority of simulations in Figure 2 fall inside the red envelope around the theoretical scaling. This indicates that the remaining differences between theory and simulations can be in largely explained by a factor-of-two inaccuracy in the derivation. One potential source of inaccuracy is the inefficiency factor χ , which I assumed to be constant but which could vary if the atmosphere’s heat engine efficiency shifted in response to changes in surface pressure or optical thickness. Another potential source of inaccuracy is the effect of planetary rotation. For a given planet the rotation rate is constant, so one might naively expect a roughly constant mismatch between theory and simulations. A planet’s rotation interacts with the large-scale circulation, however, to induce spatially varying flow and temperature patterns which could shift with changes in pressure or optical thickness and thus create a varying mismatch between theory and simulations.

Figure 3 shows that the scaling also captures the main trends in nightside brightness temperatures. This is not surprising - given that the theory largely captures the dayside’s thermal emission, energy conservation im-

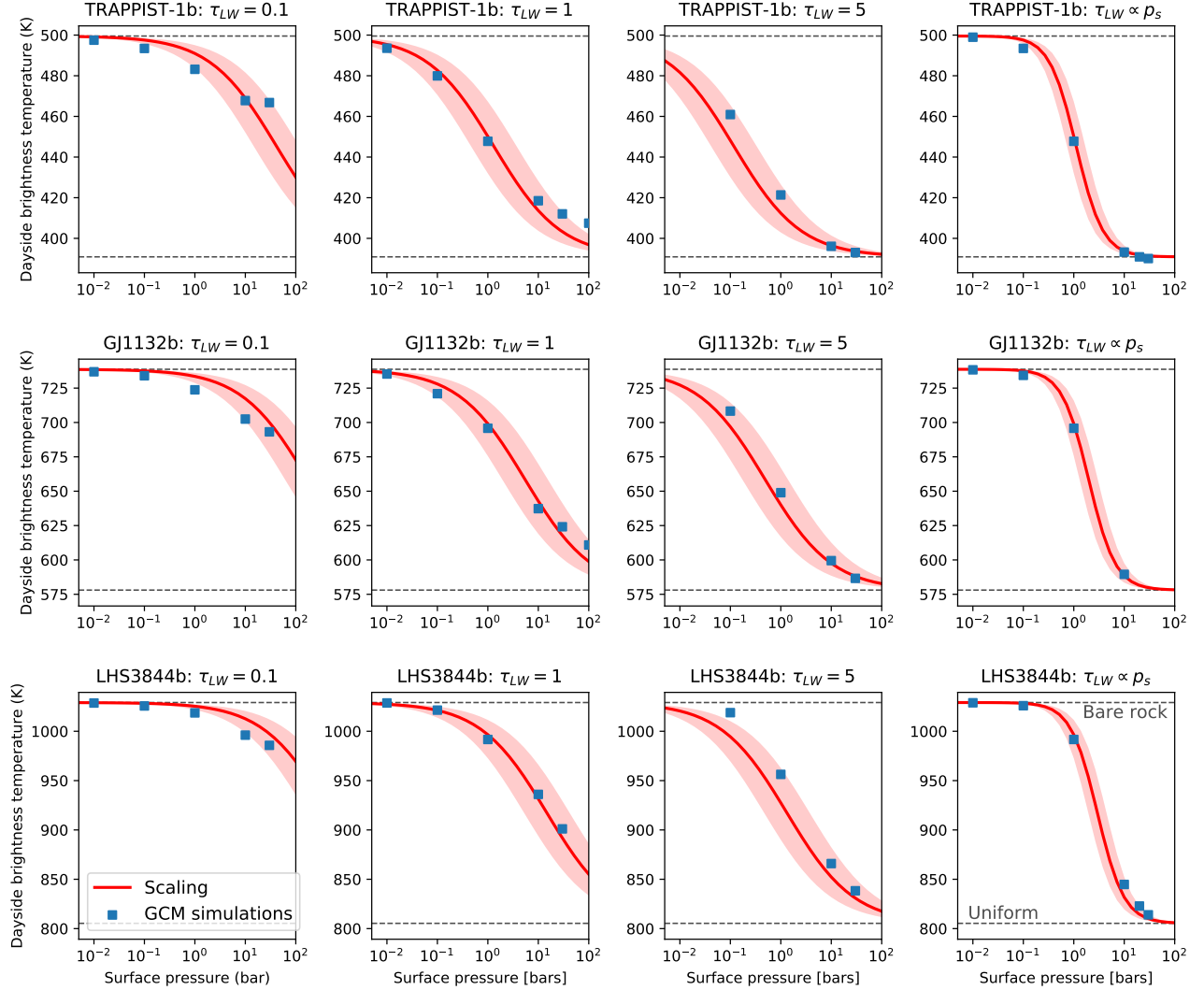


Figure 2. The theoretical scaling captures how a planet’s dayside thermal emission depends on atmospheric and planetary parameters. Dots are GCM simulations, the red line is the theoretical scaling, and the light red envelope indicates a representative factor of two uncertainty in the heat engine efficiency parameter that enters the theory. Horizontal dashed lines show the limiting cases of a bare rock (zero heat redistribution) and uniform redistribution.

plies that the theory should match the nightside thermal emission with similar accuracy. As on the dayside, the majority of nightside brightness temperatures agree with the scaling to within a factor of two change in k . This means the theory is able to predict both a planet’s dayside and nightside thermal emission, which is important because one or both of these quantities can be directly measured via secondary eclipse and thermal phase curve observations.

4. ASSIGNING AN EQUIVALENT GREY OPTICAL THICKNESS

Up to now I have assumed grey radiative transfer, but real gases have an optical thickness that varies strongly as a function of wavelength. How can one assign an equivalent optical thickness τ_{LW} to atmospheres with realistic compositions? I tested Rosseland and Planck mean opacities but found that they provide a poor fit. Instead I propose a solution here which correctly captures the degree to which an atmosphere diminishes the surface’s thermal emission, and thus reduces a planet’s observable surface emission below that of a bare rock.

For an atmosphere with spectrally varying absorption, the planet’s top-of-atmosphere thermal flux is equal to

$$F = \pi \int B_{\lambda}(T_s) e^{-\tau_{\lambda}} d\lambda + (\text{atm. emission}). \quad (10)$$

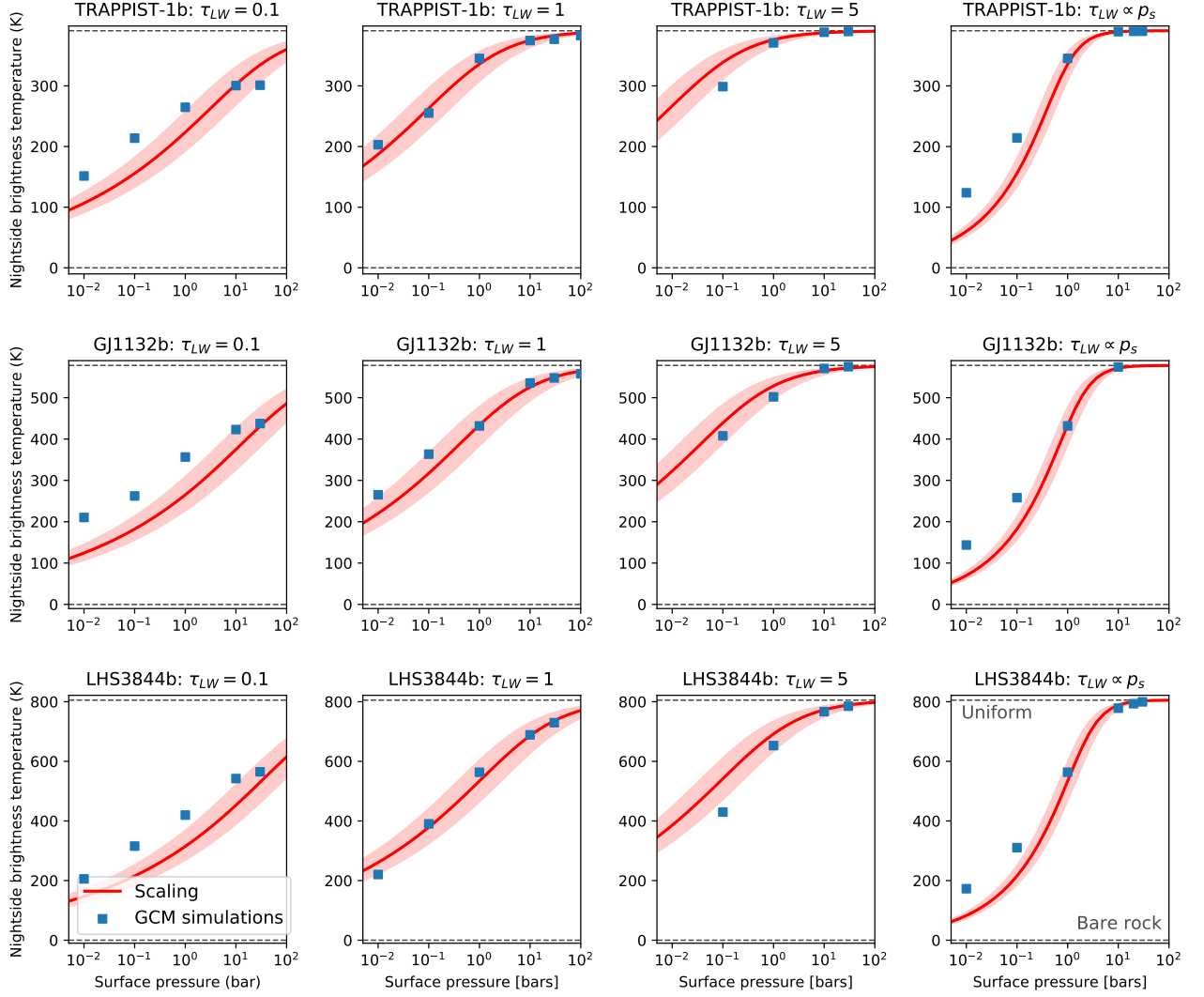


Figure 3. The theoretical scaling captures how a planet’s nightside thermal emission depends on atmospheric and planetary parameters. Dots are GCM simulations, the red line is the theoretical scaling, and the light red envelope indicates a representative factor of two uncertainty in the heat engine efficiency parameter that enters the theory. Horizontal dashed lines show the limiting cases of a bare rock (zero heat redistribution) and uniform redistribution.

Here λ is wavelength, T_s is the surface temperature, the first term is the surface’s blackbody emission attenuated by the overlying atmosphere, and the second term is the atmosphere’s emission. For comparison, with a grey absorber the top-of-atmosphere thermal flux is equal to

$$F = \sigma T_s^4 e^{-\tau_{LW}} + (\text{atm. emission}), \quad (11)$$

where τ_{LW} is now the atmosphere’s grey optical thickness.

By setting the two surface terms equal to each other, one can define the equivalent grey optical thickness for any atmospheric composition as

$$\tau_{LW} \equiv -\ln \left[\frac{\int e^{-\tau_\lambda} B_\lambda(T_s) d\lambda}{\int B_\lambda(T_s) d\lambda} \right]. \quad (12)$$

This equivalent grey optical thickness has the desirable property that it exactly matches the extent to which an atmospheric column attenuates the surface’s thermal flux. It is therefore most appropriate for the thin-atmosphere limit, in which most of a planet’s thermal emission originates at the surface, and it correctly captures how the gradual increase of atmospheric mass then reduces the planet’s surface thermal emission below that of a bare rock.

Figure 4 shows τ_{LW} for four representative atmospheric compositions, namely pure CO_2 , H_2O , O_3 , and CO . To calculate τ_{LW} I use a 1D radiative transfer model with line-by-line spectral resolution (Koll &

Cronin 2018)². The surface temperature is set to the equilibrium temperature of LHS3844b and the overlying atmosphere follows a dry adiabat. For all molecules I use opacities from the HITRAN2016 database. I also include collision-induced absorption (CIA) data for H₂O and CO₂ using the fits from Pierrehumbert (2010). I am not aware of CO-CO or O₃-O₃ CIA data, even though they should become important at high surface pressures, so the optical thicknesses shown in Figure 4 should be treated as a lower bound.

H₂O is a very strong absorber, with 10⁻² bar of H₂O enough to make the atmosphere optically thick. Next follow CO₂ and O₃, which become optically thick once surface pressure exceeds about 1 bar. Finally, CO is the poorest absorber out of these gases, and is optically thin even at a surface pressure of 1 bar. The rate at which τ_{LW} increases with pressure can be roughly understood as follows. At low surface pressure τ_{LW} is dominated by the behavior of individual molecular absorption lines, so absorption is proportional to pressure (see strong and weak line limits in Pierrehumbert 2010). H₂O and CO both follow this expectation below about 10⁻² bar. At high surface pressures absorption becomes dominated by CIA, which scales with pressure squared. H₂O follows this expectation above 1 bar. Finally, for CO₂ and O₃, as well as CO above 0.1 bar, τ_{LW} is set by the closing of a molecule’s window regions and thus a molecule’s overall band shape. For a molecular band for which absorption decays roughly exponentially away from the band center, this implies a logarithmic scaling with pressure (Pierrehumbert 2010; Koll & Cronin 2018).

Figure 4 shows that for an atmosphere with a moderately strong greenhouse effect, such as CO₂, the equivalent optical thickness of a 1 bar atmosphere is of order unity. Combined with Equation 9, this implies that the typical surface pressure above which the thermal phase curve of a rocky exoplanet with $T_{eq} \sim 600$ K starts to deviate from that of a bare rock is about 1 bar. This approximate $\mathcal{O}(1)$ bar threshold will be smaller for cooler planets or for atmospheres with a strong greenhouse effect, such as pure H₂O, and it will be larger for a hotter planets or atmospheres with a weak greenhouse effect, such as pure CO.

5. DISCUSSION

The scaling derived here provides first-order insight into the processes that determine the day-night thermal contrasts of tidally locked, rocky exoplanets. The

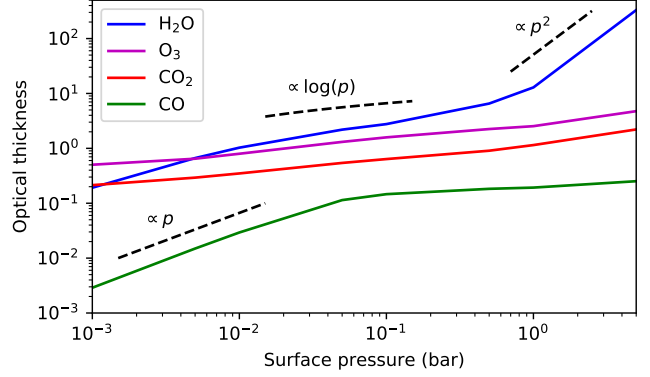


Figure 4. Equivalent grey optical thickness for actual gases. I assume an atmospheric column filled with a single gas, a dry adiabatic temperature structure, and a surface temperature representative of LHS3844b. H₂O is a strong absorber and is effectively optically thick above $\sim 10^{-2}$ bar. O₃ and CO₂ become optically thick above ~ 1 bar. The main exception is a poor absorber like CO, which is still optically thin at 1 bar.

scaling builds on the numerical results of Koll & Abbot (2015) and the theory of Koll & Abbot (2016), and translates them into observable quantities that can be measured in the near future with *JWST* via secondary eclipse and phase curve measurements.

Although the scaling relies on grey radiation for its derivation, it also appears to agree with previous GCM studies that used full radiative transfer. Selsis et al. (2011) found that the transition between large day-night contrasts and uniform emission on short-period rocky planets occurs somewhere between 0.1 and 1 bars. The scaling here agrees with their results and predicts a transition at 0.4 bar, assuming their planetary parameters and a CO₂ atmosphere with $\tau_{LW} \sim 1$. Similarly, Yang et al. (2013) and Wolf et al. (2019) simulated habitable-zone planets with 1 bar surface pressure and full H₂O thermodynamics (condensation and clouds). These studies found thermal phase curves that are fairly uniform relative to a bare rock, and thus also support the scaling here which predicts a transition at about 0.2 bar (note that the addition of full H₂O thermodynamics will tend to move the transition to even lower surface pressures, see below).

Looking towards upcoming observations with *JWST*, one outstanding issue is that the thermal emission of rocky exoplanets can be affected by additional atmospheric and planetary physics are not included here. I expect that the scaling should generally overpredict a planet’s day-night thermal contrast for the following reasons:

² Available at <https://github.com/ddbkoll/PyRADS>.

First, the theory assumes dry thermodynamics, but an atmosphere with condensation can additionally transport heat via horizontal latent heat transport (Ding & Pierrehumbert 2018). The derivation here does not capture this process, so it should tend to overpredict day-night thermal contrasts in atmospheres in which condensation starts to become important.

Second, I do not include the radiative effect of clouds. Similar to latent heating, clouds should also tend to smooth out the day-night thermal contrast on tidally locked planets. The underlying reason is that high clouds, which have the largest impact on thermal emission, tend to form via moist convection. On tidally locked planets moist convection occurs on the dayside, so convective clouds will preferentially reduce the dayside’s thermal emission. GCM simulations confirm this expectation and show that deep convective clouds can even reverse a planet’s day-night thermal contrast, such that the nightside emits more flux than the dayside (Yang et al. 2013). Subsequent work has shown that, on planets with short orbital periods, cloud cover tends to be more evenly distributed because equatorial superrotation can suppress strong vertical motion near the substellar point (Kopparapu et al. 2016; Komacek & Abbot 2019), but even in this case clouds tend to reduce, not amplify, a planet’s day-night emission contrast.

Third and finally, some exoplanets might be able to sustain a surface ocean. Unless the ocean was made out of exotic non-H₂O condensibles, these planets would have to be temperate and lie inside the habitable zone. In addition to atmospheric phase changes and clouds becoming important on such planets (see above), an ocean can additionally transport energy via its fluid motions which will again reduce the planet’s day-night thermal contrast (Yang et al. 2019).

6. CONCLUSION

I have derived an analytical scaling which captures the dominant processes that determine atmospheric day-night heat redistribution on tidally locked rocky exoplanets. The scaling compares favorably against a large set of idealized GCM simulations.

Both scaling and simulations suggest that a typical surface pressure above which broadband secondary eclipses and thermal phase curves of short-period rocky exoplanets deviate from a bare rock is $\mathcal{O}(1)$ bar, even though the exact threshold depends on additional quantities such as atmospheric composition and planetary temperature.

In addition to improving our understanding of exoplanet atmospheres, the scaling is useful in the context of

modeling and interpreting thermal observations of rocky exoplanets. For favorable targets, *JWST* will be able to measure broadband thermal fluxes as well as emission spectra (e.g., Greene et al. 2016; Morley et al. 2017; Batalha et al. 2018; Kempton et al. 2018). To make sense of these measurements, models are needed that properly account for the physical processes which shape the observable features of rocky exoplanets. The scaling derived here offers a way of parameterizing the large-scale atmospheric heat transport in 1D models, and was used as such in a number of related studies (Koll et al; Malik et al; Kreidberg et al; Mansfield et al; all submitted). Doing so is attractive because parameterization is many orders of magnitude faster than explicitly simulating an atmosphere’s large-scale fluid dynamics.

This work was supported by a James McDonnell Foundation postdoctoral fellowship. I thank Dorian Abbot and Jacob Bean for crucial discussions about *JWST* observations that sparked this paper, and for providing subsequent feedback. I also thank Tim Cronin for an insightful discussion about opacity scalings.

REFERENCES

- Batalha, N. E., Lewis, N. K., Line, M. R., Valenti, J., & Stevenson, K. 2018, *The Astrophysical Journal Letters*, 856, L34, doi: [10.3847/2041-8213/aab896](https://doi.org/10.3847/2041-8213/aab896)
- Benneke, B., & Seager, S. 2012, *The Astrophysical Journal*, 753, 100, doi: [10.1088/0004-637X/753/2/100](https://doi.org/10.1088/0004-637X/753/2/100)
- Berta-Thompson, Z. K., Irwin, J., Charbonneau, D., et al. 2015, *Nature*, 527, 204, doi: [10.1038/nature15762](https://doi.org/10.1038/nature15762)
- Burrows, A. S. 2014, *Proceedings of the National Academy of Sciences*, 111, 12601, doi: [10.1073/pnas.1304208111](https://doi.org/10.1073/pnas.1304208111)
- Chen, J., & Kipping, D. 2017, *The Astrophysical Journal*, 834, 17, doi: [10.3847/1538-4357/834/1/17](https://doi.org/10.3847/1538-4357/834/1/17)
- Cowan, N. B., & Agol, E. 2008, *The Astrophysical Journal*, 678, L129, doi: [10.1086/588553](https://doi.org/10.1086/588553)
- de Wit, J., Wakeford, H. R., Lewis, N. K., et al. 2018, *Nature Astronomy*, 2, 214, doi: [10.1038/s41550-017-0374-z](https://doi.org/10.1038/s41550-017-0374-z)
- Delrez, L., Gillon, M., Triaud, A. H. M. J., et al. 2018, *Monthly Notices of the Royal Astronomical Society*, 475, 3577, doi: [10.1093/mnras/sty051](https://doi.org/10.1093/mnras/sty051)
- Demory, B.-O., Gillon, M., de Wit, J., et al. 2016, *Nature*, 532, 207, doi: [10.1038/nature17169](https://doi.org/10.1038/nature17169)
- Diamond-Lowe, H., Berta-Thompson, Z., Charbonneau, D., & Kempton, E. M.-R. 2018, *The Astronomical Journal*, 156, 42, doi: [10.3847/1538-3881/aac6dd](https://doi.org/10.3847/1538-3881/aac6dd)
- Ding, F., & Pierrehumbert, R. T. 2018, *The Astrophysical Journal*, 867, 54, doi: [10.3847/1538-4357/aae38c](https://doi.org/10.3847/1538-4357/aae38c)
- Faucher, T., Arney, G., Kopparapu, R. K., & Goldman, S. D. 2018, *geosciences* 2018, Vol. 4, Pages 180-191, doi: [10.3934/geosci.2018.4.180](https://doi.org/10.3934/geosci.2018.4.180)
- Feng, Y. K., Line, M. R., Fortney, J. J., et al. 2016, *The Astrophysical Journal*, 829, 52, doi: [10.3847/0004-637X/829/1/52](https://doi.org/10.3847/0004-637X/829/1/52)
- Frierson, D. M. W., Held, I. M., & Zurita-Gotor, P. 2006, *Journal of the Atmospheric Sciences*, 63, 2548, doi: [10.1175/JAS3753.1](https://doi.org/10.1175/JAS3753.1)
- Gillon, M., Jehin, E., Lederer, S. M., et al. 2016, *Nature*
- Greene, T. P., Line, M. R., Montero, C., et al. 2016, *The Astrophysical Journal*, 817, 17, doi: [10.3847/0004-637X/817/1/17](https://doi.org/10.3847/0004-637X/817/1/17)
- Heng, K., Menou, K., & Phillipps, P. J. 2011, *Monthly Notices of the Royal Astronomical Society*, 413, 2380, doi: [10.1111/j.1365-2966.2011.18315.x](https://doi.org/10.1111/j.1365-2966.2011.18315.x)
- Hörst, S. M., He, C., Lewis, N. K., et al. 2018, *Nature Astronomy*, 2, 303, doi: [10.1038/s41550-018-0397-0](https://doi.org/10.1038/s41550-018-0397-0)
- Hu, R., & Seager, S. 2014, *The Astrophysical Journal*, 784, 63, doi: [10.1088/0004-637X/784/1/63](https://doi.org/10.1088/0004-637X/784/1/63)
- Joshi, M., Haberle, R., & Reynolds, R. 1997, *Icarus*, 129, 450, doi: [10.1006/icar.1997.5793](https://doi.org/10.1006/icar.1997.5793)
- Kaspi, Y., & Showman, A. P. 2015, *The Astrophysical Journal*, 804, 60, doi: [10.1088/0004-637X/804/1/60](https://doi.org/10.1088/0004-637X/804/1/60)
- Kempton, E. M.-R., Lupu, R., Owusu-Asare, A., Slough, P., & Cale, B. 2017, *Publications of the Astronomical Society of the Pacific*, 129, 044402, doi: [10.1088/1538-3873/aa61ef](https://doi.org/10.1088/1538-3873/aa61ef)
- Kempton, E. M.-R., Bean, J. L., Louie, D. R., et al. 2018, *Publications of the Astronomical Society of the Pacific*, 130, 114401, doi: [10.1088/1538-3873/aadf6f](https://doi.org/10.1088/1538-3873/aadf6f)
- Koll, D. D. B., & Abbot, D. S. 2015, *The Astrophysical Journal*, 802, 21, doi: [10.1088/0004-637X/802/1/21](https://doi.org/10.1088/0004-637X/802/1/21)
- . 2016, *The Astrophysical Journal*, 825, 99, doi: [10.3847/0004-637X/825/2/99](https://doi.org/10.3847/0004-637X/825/2/99)
- Koll, D. D. B., & Cronin, T. W. 2018, *Proceedings of the National Academy of Sciences*, 201809868, doi: [10.1073/pnas.1809868115](https://doi.org/10.1073/pnas.1809868115)
- Koll, D. D. B., & Komacek, T. D. 2018, *The Astrophysical Journal*, 853, 133, doi: [10.3847/1538-4357/aaa3de](https://doi.org/10.3847/1538-4357/aaa3de)
- Komacek, T. D., & Abbot, D. S. 2019, *The Astrophysical Journal*, 871, 245, doi: [10.3847/1538-4357/aafb33](https://doi.org/10.3847/1538-4357/aafb33)
- Kopparapu, R. K., Wolf, E. T., Haqq-Misra, J., et al. 2016, *The Astrophysical Journal*, 819, 84, doi: [10.3847/0004-637X/819/1/84](https://doi.org/10.3847/0004-637X/819/1/84)
- Line, M. R., & Parmentier, V. 2016, *The Astrophysical Journal*, 820, 78, doi: [10.3847/0004-637X/820/1/78](https://doi.org/10.3847/0004-637X/820/1/78)
- Line, M. R., Wolf, A. S., Zhang, X., et al. 2013, *The Astrophysical Journal*, 775, 137, doi: [10.1088/0004-637X/775/2/137](https://doi.org/10.1088/0004-637X/775/2/137)
- Liu, Y., Wu, W., Jensen, M. P., & Toto, T. 2011, *Atmospheric Chemistry and Physics Discussions*, 11, 5681, doi: [10.5194/acpd-11-5681-2011](https://doi.org/10.5194/acpd-11-5681-2011)
- Madhusudhan, N., & Seager, S. 2009, *The Astrophysical Journal*, 707, 24, doi: [10.1088/0004-637X/707/1/24](https://doi.org/10.1088/0004-637X/707/1/24)
- Merlis, T. M., & Schneider, T. 2010, *Journal of Advances in Modeling Earth Systems*, 2, doi: [10.3894/JAMES.2010.2.13](https://doi.org/10.3894/JAMES.2010.2.13)
- Mills, S. M., & Abbot, D. S. 2013, *The Astrophysical Journal Letters*, 774, L17, doi: [10.1088/2041-8205/774/2/L17](https://doi.org/10.1088/2041-8205/774/2/L17)
- Moran, S. E., Hörst, S. M., Batalha, N. E., Lewis, N. K., & Wakeford, H. R. 2018, arXiv:1810.05210 [astro-ph]. <https://arxiv.org/abs/1810.05210>
- Morley, C. V., Kreidberg, L., Rustamkulov, Z., Robinson, T., & Fortney, J. J. 2017, *The Astrophysical Journal*, 850, 121, doi: [10.3847/1538-4357/aa927b](https://doi.org/10.3847/1538-4357/aa927b)
- Moses, J. I., Visscher, C., Fortney, J. J., et al. 2011, *The Astrophysical Journal*, 737, 15, doi: [10.1088/0004-637X/737/1/15](https://doi.org/10.1088/0004-637X/737/1/15)

- Pierrehumbert, R. T. 2010, *Principles of Planetary Climate* (Cambridge, UK: Cambridge University Press)
- . 2011, *The Astrophysical Journal*, 726, L8, doi: [10.1088/2041-8205/726/1/L8](https://doi.org/10.1088/2041-8205/726/1/L8)
- Robinson, T. D., & Catling, D. C. 2014, *Nature Geoscience*, 7, 12, doi: [10.1038/ngeo2020](https://doi.org/10.1038/ngeo2020)
- Seager, S., & Sasselov, D. D. 2000, *The Astrophysical Journal*, 537, 916, doi: [10.1086/309088](https://doi.org/10.1086/309088)
- Selsis, F., Wordsworth, R. D., & Forget, F. 2011, *Astronomy and Astrophysics*, 532, 1, doi: [10.1051/0004-6361/201116654](https://doi.org/10.1051/0004-6361/201116654);
- Tinetti, G., Liang, M.-C., Vidal-Madjar, A., et al. 2007, *The Astrophysical Journal Letters*, 654, L99, doi: [10.1086/510716](https://doi.org/10.1086/510716)
- Vanderspek, R., Huang, C. X., Vanderburg, A., et al. 2019, *The Astrophysical Journal*, 871, L24, doi: [10.3847/2041-8213/aafb7a](https://doi.org/10.3847/2041-8213/aafb7a)
- Wolf, E. T., Kopparapu, R. K., & Haqq-Misra, J. 2019, *The Astrophysical Journal*, 877, 35, doi: [10.3847/1538-4357/ab184a](https://doi.org/10.3847/1538-4357/ab184a)
- Wordsworth, R. 2015, *The Astrophysical Journal*, 806, 180
- Yang, J., Abbot, D. S., Koll, D. D. B., Hu, Y., & Showman, A. P. 2019, *The Astrophysical Journal*, 871, 29, doi: [10.3847/1538-4357/aaf1a8](https://doi.org/10.3847/1538-4357/aaf1a8)
- Yang, J., Cowan, N. B., & Abbot, D. S. 2013, *The Astrophysical Journal Letters*, 771, L45, doi: [10.1088/2041-8205/771/2/L45](https://doi.org/10.1088/2041-8205/771/2/L45)